Solid State Science and Technology, Vol. 23, No 1 & 2 (2015) 90-98
ISSN 0128-7389 | *http://journal.masshp.net*

THE ELECTROCHEMICAL PERFORMANCE OF SUGAR-DERIVED ORDERED MESOPOROUS CARBON ELECTRODE

Nur Izzatie Hannah Razman[1,2], Salasiah Endud[1,], Zainab Ramli[1] and Izan Izwan Misnon[3]

[1]*Department of Chemistry, Faculty of Science, Universiti Teknologi Malaysia, 81310 UTM Johor Bahru, Johor, Malaysia*

[2]*Faculty of Applied Sciences, Universiti Teknologi MARA, 40450 Shah Alam, Selangor, Malaysia*

[3]*Nanostructured Renewable Energy Materials Laboratory, Faculty of Industrial Sciences & Technology, Universiti Malaysia Pahang, 26300 Kuantan, Pahang*

Corresponding author: izzatihanna@yahoo.com.my

ABSTRACT

Sugar-derived ordered mesoporous carbon, OMC was prepared by infiltration of sugar into the porosity of SBA-15 template followed by carbonization in an inert ambience. The structure, porosity and surface characteristics of the OMC were evaluated using XRD, TEM and nitrogen physisorption analysis. The OMC obtained as replica of SBA-15 template possesses high BET surface area (~900 m^2g^{-1}), pore size distribution in mesopores range and large pore volume (0.93 cm^3g^{-1}). The electrochemical performance of the material in 1 M KOH aqueous electrolyte was investigated by cyclic voltammetry (CV), galvanostatic charge-discharge (CD) and electrochemical impedance spectroscopy (EIS). The influence of scan rate and current density were evaluated. The results showed high specific capacitance and good capacitance retention over high scan rate and current density. The OMC can be used as alternative electrode material in EDLC and supercapacitor application.

Keywords: Electrochemical; ordered mesoporous carbon; SBA-15; sugar; template

INTRODUCTION

There has been tremendous interest in the development of ordered mesoporous carbon (OMC) owing to its ordered pore structure, high surface area, large pore volume, chemical inertness, high mechanical stability and conductivity [1–2]. The OMC becomes promising electrode material for high performance electrochemical capacitor due to its well-aligned mesopore system (2–50 nm) that acts as highway for smooth electron and ions transportation [3]. It also has been demonstrated that the application of OMC is strongly influenced not only by its structural properties, but also by its surface functionalities [4–5]. Oxygen surface functionalities (*e.g.*, carboxylic acid, carbonyl, and hydroxyl) are able to increase the carbon surface wettability in aqueous

electrolyte thus leads to improvement of electrochemical capacitance.

OMC can be prepared via nano-casting method which allows easy control of the structure and morphology [5]. Generally, nano-casting method is a process in which template with relevant nano-scale structure, is impregnated with carbon precursor, and the initial template is subsequently removed [6]. The resulting carbon exhibit similar criteria to the template with variable three dimensional framework structures such as cubic and hexagonal, depending on the structure of the template. In other words, OMC prepared is a replicate of the template. In this study, OMC was prepared using SBA-15 as a template and sugar as a carbon source, subsequently carbonized at 800 °C for 1 h in an inert ambience. The OMC was characterized with respect to its morphological and structural properties. The objective of this study is to evaluate the electrochemical performance of sugar-derived OMC in various scan rate and current density.

EXPERIMENTAL

Synthesis of SBA-15 template. SBA-15 was prepared according to the procedure described by Zhao *et al.* [7]. Pluronic P123 was cast off the as-synthesize product using a 200 mL Soxhlet extractor in ethanol–water mixture (50 wt.%) for 18 h.

Synthesis of sugar-derived OMC. OMC was synthesized according to the procedure described elsewhere [8]. The final product obtained was carbonized at 800 °C for 1 h in an inert ambience. The carbon/SBA-15 composite was treated with HF solution (10 wt.%) to remove the SBA-15.

Characterization of OMC. The structural properties of the OMC were evaluated by using nitrogen physisorption analyser, X-ray diffraction (XRD), Field Emission Scanning Electron Microscopy (FESEM), and Transmission Electron Microscopy (TEM).

Electrode preparation. The electrode were prepared by mixing the OMC (70 wt.%) with carbon (Super P, 15 wt.%) and PVDF binder (15 wt.%) using NMP as a solvent. The mixture was stirred for 24 h and thereby coated onto a pre-cleaned Ni foam substrate. The coated electrode was heated at 60 °C for 24 h and finally pressed at 5 MPa using a hydraulic press.

Electrochemical studies. The CV were obtained in the potential range of –1.0–0.0 V at various scan rates using a potentiostat (Autolab PGSTAT 30, Eco Chemie B.V., The Netherlands). CD was obtained by cycling the potential from –1.0 to 0.0 V with different current densities. The EIS analysis was studied in the frequency range 20 kHz to 10 mHz at bias potential of 10 mV.

RESULTS AND DISCUSSION

Physicochemical characterization of OMC. The porous structure of SBA-15 and OMC was evaluated from nitrogen physisorption measurement. The nitrogen adsorption–desorption isotherms of SBA-15 and OMC as illustrated in Figure 1(a), described typical type IV profile which is a characteristic of mesoporous material [9]. This phenomenon is associated with capillary condensation in mesopores commenced at relative pressure > 0.42. Additionally, after replication, the BET isotherm studies show increased in specific surface area (S_{BET}) from 498.20 m^2g^{-1} (SBA-15) to 899.30 m^2g^{-1} (OMC) and total pore volume from 0.70 cm^3g^{-1} (SBA-15) to 0.93 cm^3g^{-1} (OMC) (seen in Table 1). All samples showed different type of hysteresis loop which corresponds to different specific pore structures. SBA-15 shows H1 type hysteresis indicated fairly regular array uniform sphere of porous silica materials and narrow pore size distribution. OMC showed type H3 hysteresis which does not exhibit any limiting adsorption at high P/P_o, representing aggregates of carbon particles with slit-shape pores [9]. Other structural parameters of SBA-15 and OMC were also evaluated from their pore size distributions (Figure 1(b)). The pore volume broad peaks centred at 5.6 nm and 4.1 nm for SBA-15 and OMC respectively, suggests that the pore volumes are predominantly composed of mesopores and concentrated in a relatively wide size range.

Table 1: The structural parameters of the SBA-15 and OMC

Sample	*d*-spacing (nm)	[a] a_o (nm)	[b] S_{BET} (m^2g^{-1})	[c] V_{total} (cm^3g^{-1})	[d] V_{meso} (cm^3g^{-1})	[e] V_{micro} (cm^3g^{-1})	[f] d_{BJH} (nm)
SBA-15	8.64	9.98	498.20	0.70	0.65	0.05	5.60
OMC	8.46	9.77	899.30	0.93	0.61	0.32	4.10

[a] $a_o = 2d_{100}/\sqrt{3}$
[b] Surface area determined from multi point BET analysis.
[c] The pore volume at $P/P_o = 0.97$.
[d] From the difference between the pore volume at $P/P_o = 0.97$ and V_{micro}.
[e] From *t* plot (Harkins–Jura equation).
[f] Calculated from desorption branch of the isotherm by BJH method.

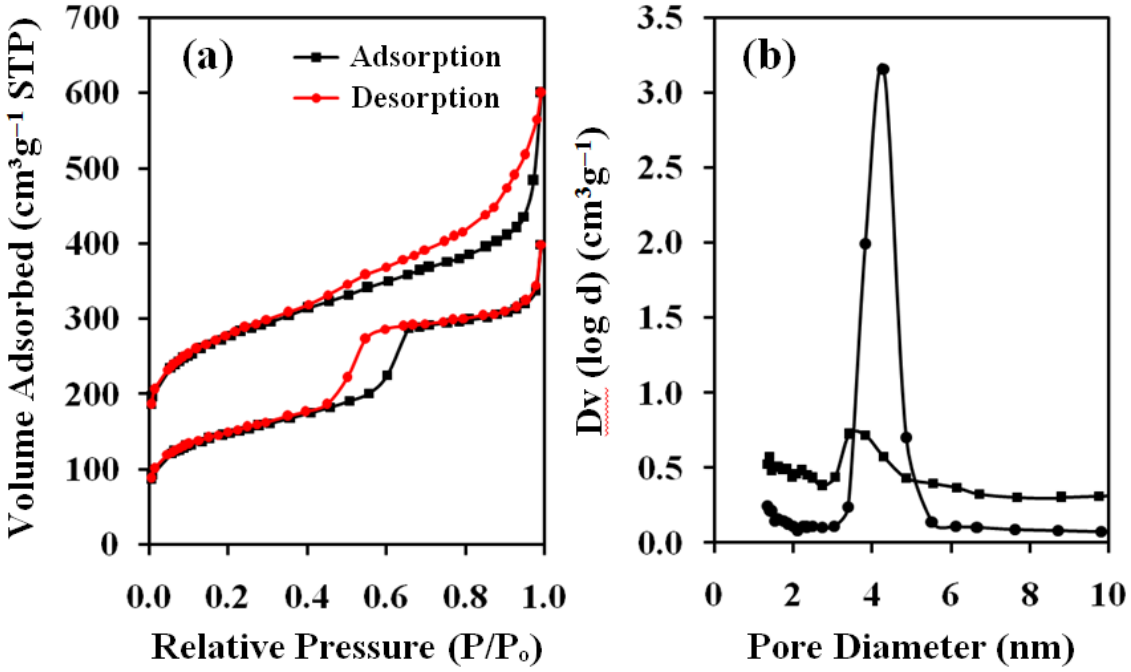

Figure 1: The nitrogen adsorption–desorption isotherms (a) and pore size distribution (b) of SBA-15 and OMC

Figure 2 shows the XRD patterns of SBA-15 and OMC. SBA-15 exhibits three diffraction lines that can be indexed to (1 0 0), (1 1 0) and (2 0 0) reflections of 2D-hexagonal space group *p*6*mm*. SBA-15 possesses a hexagonally ordered mesostructure. For OMC, only one peak corresponds to (1 0 0) plane can be distinguished. The topology of OMC has changed as the polymer undergoes a substantial volume contraction and pore size narrowing and/or broadening during high temperature carbonization. This is similar to reported by Ignat and Popovici [10] who have also obtained ordered mesoporous carbon, CMK-3 with less resolved (1 1 0) and (2 0 0) reflection peaks. The *d*-spacing and a_o values of SBA-15 and OMC are listed in Table 1.

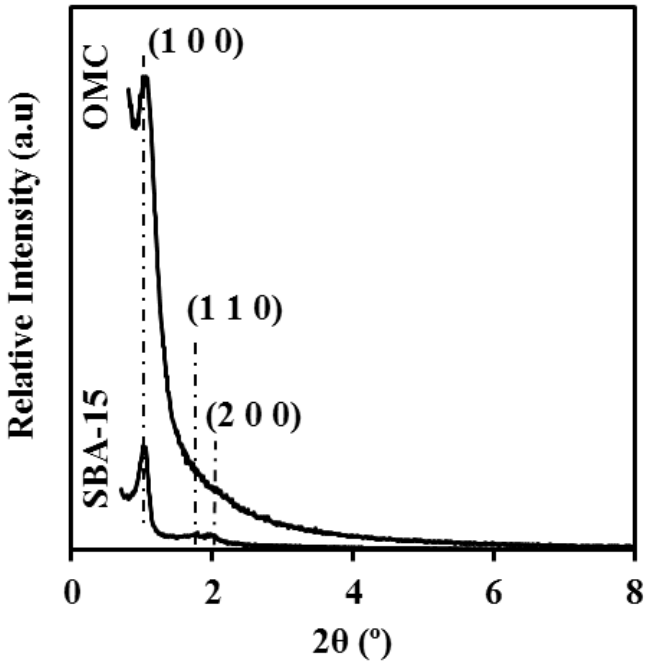

Figure 2: The XRD patterns of SBA-15 and OMC

Figure 3(a) and 3(b) are FESEM images of SBA-15 and OMC. The images demonstrate short rod-like particles shape with average length of 800–900 nm and 600–700 nm for SBA-15 and OMC, respectively. After replication process, OMC retained the rod-like particle shape morphology of SBA-15, similar to reported by previous study [11–12]. In addition, TEM image of the OMC shown in Figure 3(c) exposed the presence of well-aligned mesopores channels with average width of less than 5 nm. From the microscopic images, it is confirm that the structure of all samples is consistent with the nitrogen physisorption analysis and XRD data.

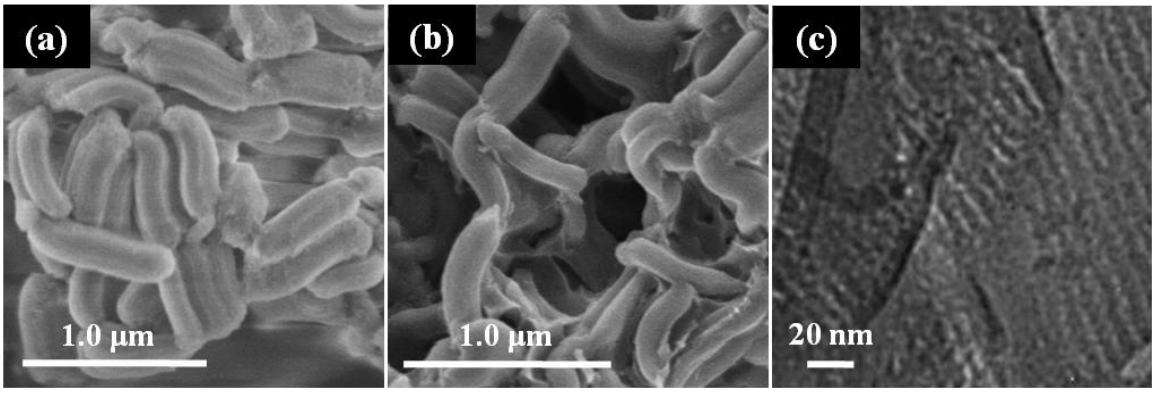

Figure 3: The FESEM images of SBA-15 (a), OMC (b); and TEM image of OMC (c)

Electrochemical analysis.
The electrochemical performance of OMC was investigated using cyclic voltammetry, CV at various scan rates (25, 50, 75, 100, 150, and 200 mVs^{-1}) and the specific capacitance, C_S was calculated according to following equation:

$$C_S = \frac{1}{2mv(E_2 - E_1)} \int_{E_1}^{E_2} i(E)dE \quad . \qquad (1)$$

where *m*, *v*, E_2, E_1, and *i(E)* are sample mass, scan rate, higher potential cutoff, lower potential cutoff and current, respectively. Figure 4(a) shows CV profile of OMC electrode in 1 M KOH aqueous electrolyte. The profile comprises a series of well-defined quasi-reversible peak pairs, indicating electric double-layer capacitor performance. As the scan rates rises, both peak currents and peak-to-peak separation increased. The curves are able to preserve near rectangular shapes as maximum scan rate (200 mVs^{-1}) is achieved, suggesting a highly reversible fast charging and discharging process. There is no redox peak observed in any of the CV curves. From 25, 50, 75, 100, 150, and 200 mVs^{-1} curves, the calculated C_S are 117, 113, 108, 103, 93, and 82 Fg^{-1}, respectively. The highest C_S value observed for OMC electrode was 117 Fg^{-1}. The results showed that the OMC electrode has relatively high specific capacitance and good capacitance retention (70%).

Electrochemical impedance spectroscopy (EIS) is a powerful technique to investigate capacitive behavior of OMC electrode. The electrochemical behavior testing was carried out using platinum as a counter electrode and Ag/AgCl as a reference electrode. The Nyquist impedance plot of the OMC electrode is presented in Figure 4(b). The plot exhibits two distinct parts, a semicircle in the high frequency region and a slope line in the low frequency region. Inset picture (Figure 4(c)) shows a clear semicircle in high frequency region. The semicircle is attributable to the process at electrode/electrolyte interface. Equivalent series resistance which corresponds to intercept of the Z' axis was measured to be 1.3 Ω. The slope line in the low frequency region is nearly vertical to the Z" axis of the spectrogram, which indicates that OMC electrode exhibits good electrochemical capacitance behavior [13].

Charge-discharge analysis was conducted in various current densities for 1000 cycles. The C_S value was calculated using relation as follows:

$$C_S = \frac{it}{m\Delta V} \quad . \qquad (2)$$

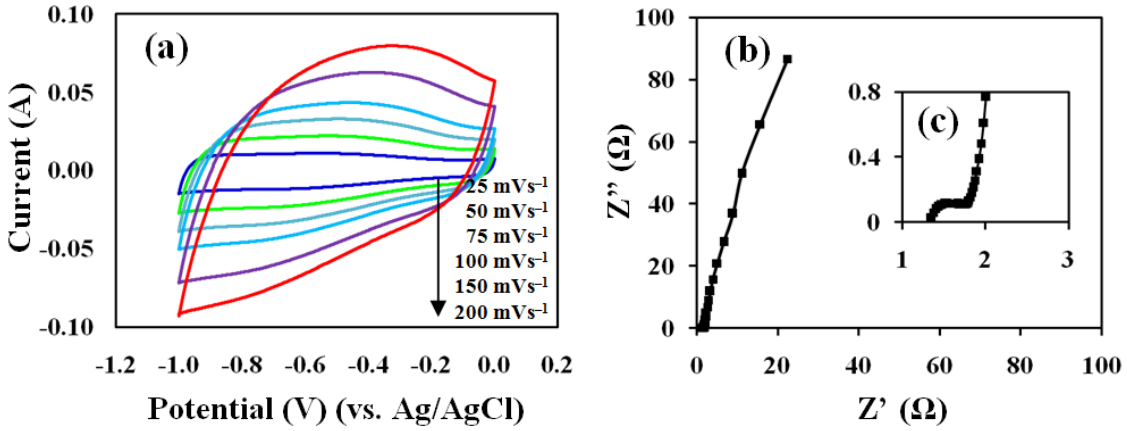

Figure 4: Cyclic voltammograms of OMC at (inner to outer) 25, 50, 75, 100, 150, and 200 mVs^{-1} (a) and Nyquist plot (b). The inset (c) shows the high frequency region of impedance

where *i*, *t*, m, and ΔV are applied current, discharge time, material mass, and open potential, respectively. This analysis is important to determine specific capacitance retention of OMC electrode in order for the electrode to work steadily and safely. Figure 5(a) shows the specific capacitance of OMC electrode at 0.3, 0.5, 1, 3, and 5 Ag^{-1}. The calculated specific capacitance is 205, 168, 147, 130, and 124 Fg^{-1}, respectively. It can be seen that the values of C_S of OMC electrode are strongly dependent on the current density. Specifically, the specific capacitance decreases with the increase of current density. Both OMC electrode and 1 M KOH electrolyte could not form electric double–layer effectively because of faster charging and discharging rate at high current density [14]. Besides, at highest current density (5 Ag^{-1}) the specific capacitance retained 60% of its initial value.

Figure 5(b) shows charge-discharge curves of the OMC electrode at 0.3, 0.5, 1, 3, and 5 Ag^{-1}. All curves exhibit symmetrical triangle shape distribution which means that this electrode has good double–layer electrochemical capability. OMC electrode experienced longer discharge time at 0.3 Ag^{-1} compared to 5 Ag^{-1}, indicating higher specific capacitance value at lower current density.

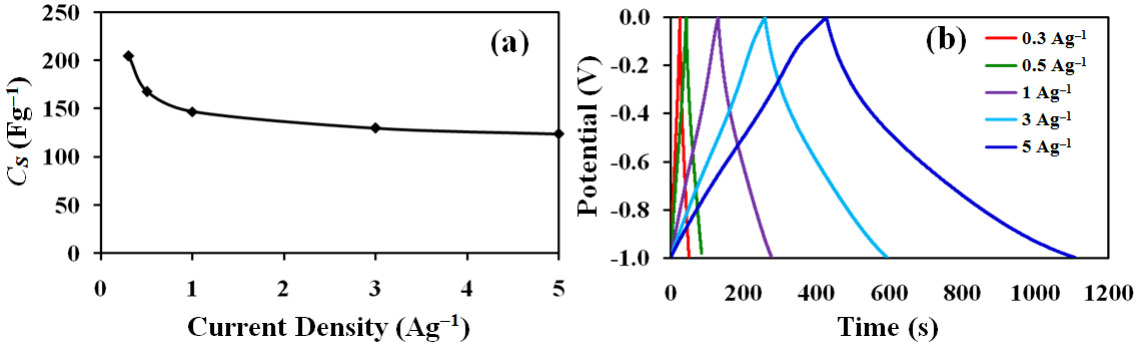

Figure 5: The specific capacitance (C_S) of OMC as a function of discharging current density (a) and charge-discharge curves of OMC at 0.3, 0.5, 1, 3, and 5 Ag^{-1} (b)

CONCLUSION

In summary, sugar-derived OMC was successfully synthesized. The OMC electrode possesses good electrochemical behavior due to constant current charge-discharge, well-defined rectangular CV profiles, and almost ideal EIS spectra. In addition, the OMC electrode is stable up to 1000 cycles.

ACKNOWLEDGEMENT

The authors acknowledge Universiti Teknologi Malaysia for research facilities, Ministry of Education (MOE, Malaysia) for financial support through GUP grant (Q.J130000.2513.05H20) and Universiti Teknologi MARA for studentship for Nur Izzatie Hannah Razman.

REFERENCES

[1]. X. Wu, X. Hong, J. Nan, Z. Luo, Q. Zhang, L. Li, H. Chen, K.S. Hui, *Microporous and Mesoporous Materials* **160** 25–31 (2012)
[2]. T. Matsui, S. Tanaka, Y. Miyake, *Advanced Powder Technology* **24** 737–742 (2013)
[3]. X. Wu, X. Hong, Z. Luo, K.S. Hui, H. Chen, J. Wu, K.N. Hui, L. Li, J. Nan, Q. Zhang, *Electrochimica Acta* **89** 400–406 (2013)
[4]. X. Zhao, Q. Zhang, B. Zhang, C-M Chen, J. Xu, A. Wang, D. S. Su, T. Zhang, *RSC Adv.* **3** 3578 (2013)
[5]. V.K. Saini, M. Andrade, M.L. Pinto, A.P. Carvalho, J. Pires, *Separation and Purification Technology* **75** 366 (2010)
[6]. K.P. Gierszal, M. Jaroniec, T-W Kim, J. Kim, R. Ryoo, *New J. Chem.* **32** 981–993 (2008)
[7]. D. Zhao, Q. Huo, J. Feng, B.F. Chmelka, G.D. Stucky, *J. Am. Chem. Soc.* **120** 6024–6036 (1998)
[8]. Ryoo, S.H. Joo, S. Jun, *J. Phys. Chem. B* **103** 7743–7746 (1999)
[9]. K.S.W. Sing, D.H. Everett, R.A.W. Haul, L. Moscou, R.A. Pierotti, J.

Rouquerol, T. Siemieniewska, *Pure & Appl. Chem.* **57** 603–619 (1985)
[10]. M. Ignat, E. Popovici, *Rev. Roum. Chim.* **56** 947–952 (2011)
[11]. A. Vinu, P. Srinivasu, M. Takahashi, T. Mori, V.V. Balasubramanian, K. Ariga, *Microporous and Mesoporous Materials* **100** 20–26 (2007)
[12]. A. Fallah, D. Kordestani, A. Alizadeh, S. Endud, *Advanced Materials Research* **622–623** 757–761 (2013)
[13]. H. Luo, F. Zhang, X. Zhao, Y. Sun, K. Du, H. Feng, *J Mater Sci: Mater Electron* **25** 538–545 (2014)
[14]. X. Zhai, J. Liu, P. Li, M. Zhong, C. Ma, H. Wang, Q. Guo, Y. Song, L. Zhi, *Int. J. Electrochem. Sci.* **7** 7304–7312 (2012)